

An Experimental Study on the Out-Of-Plane Stability of Reinforced Masonry Shear Walls Under In-Plane Reversed Cyclic Loads



15 WCEE
LISBOA 2012

N. Azimikor, B. Robazza, K. Elwood, and D. L. Anderson

University of British Columbia, Vancouver, BC, Canada

S. Brzev

British Columbia Institute of Technology, Burnaby, BC, Canada

SUMMARY:

This paper presents results of an ongoing two-phase experimental research program on the out-of-plane instability of reinforced masonry (RM) shear walls under seismic loading. Phase 1 involves testing of five reinforced masonry uniaxial specimens under reversed cyclic tension and compression. The specimens represented the end zone of a RM shear wall. The purpose of the testing was to gain insight into the factors influencing out-of-plane instability. The design parameters considered in the study include longitudinal reinforcement ratio and height-to-thickness (h/t) ratio. An analytical model was proposed to estimate the magnitude of critical tensile strain leading to out-of-plane instability. Phase 2 involves experimental and analytical study of full-scale RM shear wall specimens subjected to reversed-cyclic lateral loading, with the main objective to develop a rational analysis procedure and criteria for assessing the out-of-plane stability of these walls. This paper presents the results of Phase 1 experimental study and explains the Phase 2 experimental program.

Keywords: Reinforced masonry, Shear wall, Seismic resistance, Out-of-plane stability

1. INTRODUCTION

Reinforced masonry (RM) shear walls constructed using hollow concrete blocks reinforced with vertical and horizontal steel bars can provide a high degree of seismic protection to buildings. However, design applications of low-rise RM wall construction in Canada have been restricted by seismic design provisions of the Canadian masonry design standard CSA S304.1-04, as discussed by Anderson and Brzev (2009). In particular, stringent limits were placed on the height-to-thickness (h/t) ratio of ductile masonry walls (from 14 to 20). For example, using an h/t ratio of 20 and the common 200 mm concrete blocks limits the wall height to 4.0 m; this is impractical for some of the common masonry applications, such as fire halls or warehouse buildings. These restrictions were included in CSA S304.1-04 seismic provisions to prevent lateral (out-of-plane) instability of RM walls subjected to axial stresses due to gravity loads and overturning moments caused by lateral seismic loads, as shown in Figure 1.1.

A rational explanation for lateral instability of RM shear walls was originally presented by Paulay and Priestley (1993). A shear wall can experience lateral instability when the longitudinal reinforcement in its end zones is subjected to compression loads subsequent to cycles of high tensile strain. Uniformly distributed horizontal cracks form along the height of the plastic hinge region in the wall end zone during tension load cycles, and may not fully close in the subsequent compression load cycle. Due to the presence of open cracks and the residual plastic strains in the vertical reinforcement in the wall end zone, this portion of the wall becomes very flexible and susceptible to significant out-of-plane displacements under low compressive loads. However, if the cracks close before out-of-plane displacements cause instability, compressive stresses will develop in the masonry. This provides additional stiffness against lateral deformations and the onset of out-of-plane instability may be delayed or avoided altogether.

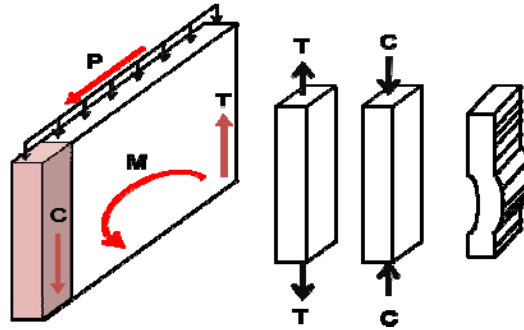


Figure 1.1. End zone of a shear wall subjected to axial tension and compression in end zones due to seismic loading

A comprehensive literature review of experimental research studies on RM shear walls subjected to in-plane reversed cyclic loads with flexure-dominant response has revealed that only a few specimens experienced the out-of-plane instability (Azimikor et al., 2011). It appears that the key design parameters that influence the out-of-plane instability include h/t ratio, height/length ratio, level of applied axial compressive stress, flexural reinforcement ratio (associated with longitudinal reinforcement), and the level of plastic strain in the reinforcement placed in the wall end zones. For example, Shedid et al. (2008) reported out-of-plane instability in rectangular wall specimens which were characterized by a high flexural reinforcement ratio (1.31 and 1.17%), while otherwise similar specimens with lower reinforcement ratios tested in the same experimental studies did not experience instability. Priestley and He (1992) reported out-of-plane instability in the web of a T-shaped RM wall specimen. Out-of-plane instability of RM shear walls was not observed in past earthquakes, however a significant damage due to out-of-plane instability of reinforced concrete shear walls was observed in a few buildings affected by the February 2010 Maule, Chile earthquake (M 8.8) and the February 2011 Christchurch, New Zealand earthquake (M 6.3).

Insufficient experimental evidence on the subject prompted the need for a research program which would characterize out-of-plane instability in RM shear walls and develop rational criteria for out-of-plane instability in these walls. This paper describes the status and findings of a four-year, two-phase experimental program which has been undertaken by the authors of this paper in November 2010. Phase 1 of the program was focused on simulating the behaviour of the wall end zones using uniaxial specimens shown shaded in Figure 1.1. Note that these specimens were not able to simulate the actual boundary conditions along the height of the wall end zone, and did not take into account the effect of the strain gradient along the wall length, however the purpose of Phase 1 study was to understand the out-of-plane instability phenomenon and identify key factors which influence its development. This paper presents the details of Phase 1 experimental study and its results, which were the scope of the Masters thesis of the first author (Azimikor 2012). Phase 2 study (currently under way) consists of testing several full-scale RM shear wall specimens under in-plane reversed cyclic loading. The test setup and status of Phase 2 study are also discussed in the paper.

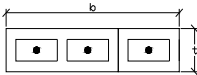
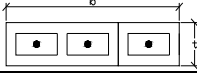
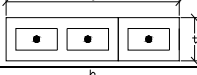
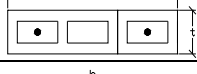
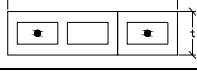
2. TESTING OF COLUMN-LIKE RM SPECIMENS UNDER UNIAXIAL REVERSED CYCLIC LOADING (PHASE 1)

2.1. Specimen Configuration and Test Setup

Phase 1 experimental program comprised of testing five full-scale block masonry uniaxial specimens (C1 to C5) representing the end zone of a RM shear wall subjected to reversed-cyclic tension and compression. Table 2.1 presents the specimen matrix and summarizes the key design parameters. All specimens were fully grouted, and had the same cross-sectional dimensions (590 mm length x 140 mm thickness). The overall height was 3.8 m; this is equivalent to 19 courses of masonry and an average 10 mm mortar bed joint thickness. The specimens were reinforced with either two or three vertical reinforcing bars of different sizes, and the reinforcement ratio was in the range of 0.24 % (similar to masonry construction practice) to 1.07% (over-reinforced, but more likely to contribute to

out-of-plane instability). Note that the reinforcing bars were placed in the centre of the specimen. Height/thickness (h/t) ratio for the specimens was equal to 27; this is significantly higher than the upper limit of 20 set by CSA S304-04. However, specimens C3 to C5 were stiffened with Glass Fiber Reinforced Polymer (GFRP) overlay. This was accomplished by applying vertical strips on the two exterior faces in the upper half of the specimen, plus two horizontal strips confining the top and bottom of the GFRP-reinforced region. The purpose of the GFRP application was to increase the stiffness of the specimens' upper portion so that tensile cracking and yielding of reinforcement are limited to the lower half. The height of the column over which tensile cracking takes place is referred to as *plastic hinge height* in this paper. Different plastic hinge heights were obtained for various specimens, due to the GFRP application on specimens C3 to C5. It can be noted from Table 2.1 that plastic hinge height is equal to the overall height (3800 mm) only for specimens C1 and C2. For specimens C3 to C5, plastic hinge height (h_p) was determined from the column deformation that resulted in tensile yielding.

Table 2.1. Specimen Matrix

Specimen	Cross section	Reinforcement	h_p^* (mm)	Notes
C1		3-15M $\rho=0.71\%$	3800	ρ is by 34% higher than that used in standard practice**
C2		3-20M $\rho=1.07\%$	3800	ρ is by 100% higher than that used in standard practice (upper bound)
C3		3-15M $\rho=0.71\%$	3462	ρ is by 34% higher than that used in standard practice; upper half reinforced with GFRP
C4		2-15M $\rho=0.48\%$	2385	ρ is close to that used in standard practice; upper half reinforced with GFRP
C5		2-10M $\rho=0.24\%$	2192	ρ is by 45% lower than standard practice and lower than the balanced ratio*** (lower bound); upper half reinforced with GFRP

Notes:

- * h_p is taken as the height over which tensile cracking takes place; note that h_p was reduced in specimens C3 to C5 due to the GFRP application.
- ** Standard practice is to provide 15M bars in cells located in the end zones of a RM shear wall built using standard 190 mm x 190 mm x 400 mm concrete masonry blocks; this is equivalent to ρ of 0.53%.
- *** Note that balanced ρ for masonry with the mechanical properties used in this test program is 0.36%.

The specimens had semi-rigid boundary conditions due to the rigid steel cap plates attached at the ends. Longitudinal reinforcing bars in each specimen were welded to these steel plates. A few models of welded connection were tested before the construction, to ensure that yielding in a reinforcing bar occurs away from the welded connection, and to avoid the weld failure. The construction was performed by threading hollow blocks from the top of the specimen, since the longitudinal reinforcement was continuous and had to be welded to the bottom plate before the construction.

The test setup was custom designed for this study, and the main objective was to ensure uniform uniaxial tension and compression stresses were applied to the specimen. The testing frame consisted of four columns and the loading beam, two double-acting MTS actuators (capacity 890 kN each) mounted vertically on either face of the specimen, and anchored to the strong floor at the bottom and to the top loading beam. Two pantographs were used to protect the setup against lateral displacements at the top while still allowing vertical movement.

The instrumentation consisted of 16 displacement transducers (linear and string potentiometers) which measured axial and lateral displacements of the specimen, as shown in Figure 2.1. Lateral displacements of the top loading beam and the supporting columns were also monitored during the testing. These transducers and the load cells attached to the actuators were connected to the data acquisition system (Digital Equipment Station).

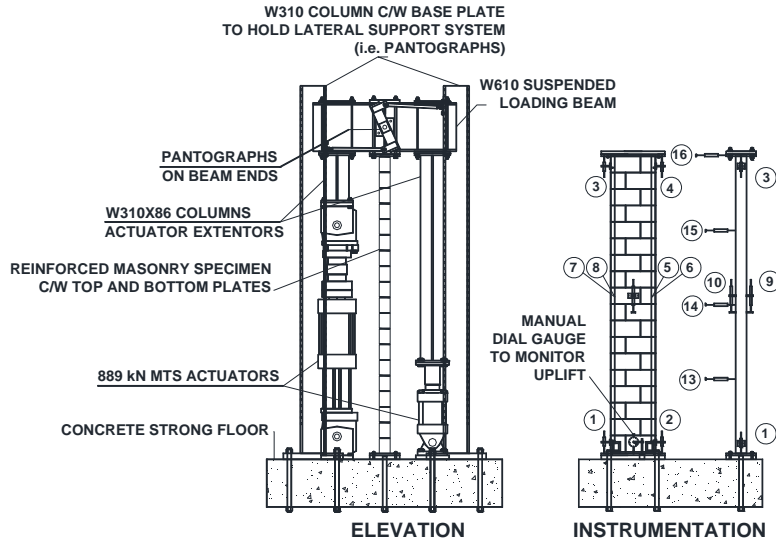


Figure 2.1. Test setup and instrumentation

2.2 Material Properties

Full-scale hollow concrete blocks with two hollow cells were used with a thickness of 140 mm, so as to get a large h/t ratio within the height constraints of the test setup. Masonry material testing was performed following the procedures outlined in pertinent Canadian standards: CSA A165-04 for block testing, and CSA A179-04 for mortar and grout testing. Average compressive strength for the blocks was 43.0 MPa for the net area, based on 9 specimens. Type S mortar was used, with the average compressive strength of 15.8 MPa (based on 18 cubes). The grout mix consisted of 1:3:2 proportion of Portland cement, sand, and aggregate by volume, with a 10 mm maximum aggregate size. The average compressive strength was 9.6 MPa (based on 4 prisms), and 17.2 MPa (based on 10 cylinders). The average masonry compressive strength, f'_m , was 22.9 MPa, based on 3 two-block-high grouted masonry prisms. In addition, 5 hollow prisms were tested, and the average strength, f'_m , was 25.8 MPa based on the net area. Grade 400 reinforcing steel with the nominal yield strength of 400 MPa was used. Tensile tests were conducted on 10M, 15M, and 20M reinforcing bar specimens in total, and the average yield strength was 584 MPa, 527 MPa, and 464 MPa respectively. The average yield strain for all specimens was 0.26%, and the strain corresponding to the onset of strain hardening was 1.5%. The specimens were prepared and tested according to CSA-G30.18-M92 (R2002) standard.

2.3 Testing Procedure

Two different loading protocols were used in the experimental program: monotonic compression loading (specimen C1) and reversed cyclic tension and compression loading (specimens C2 to C5). The test data obtained from specimen C1 was used to obtain a realistic estimate for the masonry modulus of elasticity and the compression load capacity, P_{cr} . The loading protocol for specimen C2 is shown in Figure 2.2; note that a similar loading protocol was used for specimens C3 to C5, but there were slight differences due to unique response of each specimen. Displacement control was used in tension and force control in compression. The tensile displacements were applied such that at each cycle a target multiple of the yield displacement, Δ_y , was reached. Note that Δ_y corresponds to the onset of yielding in longitudinal reinforcement estimated using the yield strain obtained from the reinforcement testing. The compression load was limited to about half the compression capacity for the specimen, $P_{cr}/2$.

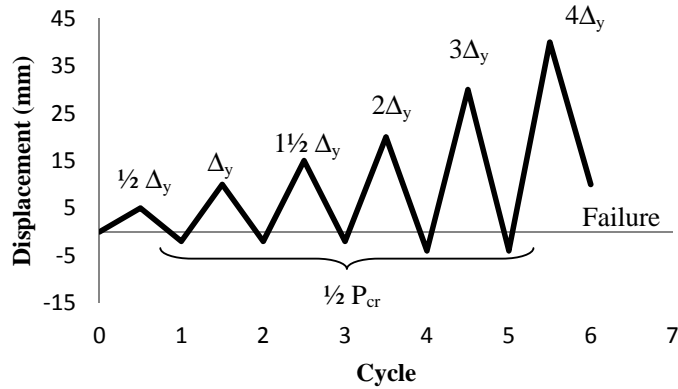


Figure 2.2. Reversed cyclic loading protocol for specimen C2

3. EXPERIMENTAL RESULTS: OBSERVED BEHAVIOUR AND FAILURE MECHANISMS

Three main failure mechanisms were observed during the testing: crushing, reinforcement buckling, and global out-of-plane instability. *Crushing* mechanism is associated with the specimen reaching its axial compression load capacity. Crushing was observed in specimen C1 which was subjected to monotonic uniaxial compression loading. It is believed that the presence of longitudinal reinforcing bars did not affect the ultimate capacity of the specimen. Specimen C1 failed at a compressive load close to 1400 kN, corresponding to a compressive strength of 17 MPa and a compressive strain of 0.12%. *Reinforcement buckling* mechanism was observed in specimen C5 with the lowest reinforcement ratio of 0.24% and the smallest bar size (10M bars with 11 mm nominal diameter). This specimen experienced significant out-of-plane displacements prior to failure, but it did not experience global instability. The bar buckling is attributed to the small bar size and a small bar surface area; this contributed to significant vertical splitting cracks and de-bonding of reinforcement in the grouted cells when the specimen was subjected to high tensile strains. *Global out-of-plane instability* was observed in specimens C2, C3, and C4. This mechanism will be explained on a generic loading cycle diagram shown in Figure 3.1. The cycle consists of a loading path *o-a'*, during which the specimen is subjected to large tensile strains, followed by an unloading path *a'-b*, and reloading of the specimen in compression. There are two general alternative scenarios for the compressive loading path: i) path *b-c-d-g-h*, when the specimen remains stable and the testing continues, or ii) the specimen experiences failure due to instability through either path *b-c-f* (global out-of-plane instability) or *b-c-d-e* (global instability combined with the localized masonry crushing).

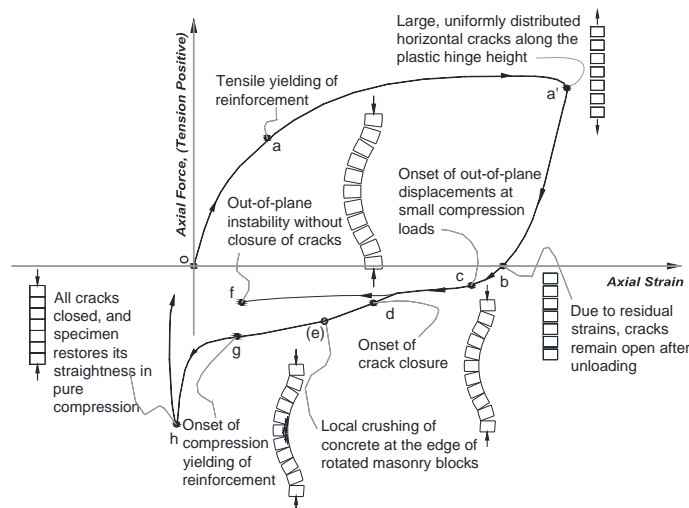


Figure 3.1. Loading cycle for a masonry specimen under cyclic tension and compression

The specimen is initially loaded in tension through path $o-a'$. Once the reinforcement has yielded (point a), the specimen experiences plastic tensile strains (and possibly strain hardening) until the end of the tension half-cycle (point a'). At that point, large uniformly distributed horizontal cracks have appeared at the masonry bed joints over the plastic hinge height, as shown in Figure 3.2a). Note that horizontal cracks in block masonry structures generally occur along horizontal bed joints.

During the unloading path $a'-b$, the reinforcing bars recover elastic strain. Once the point b (complete unload) has been reached, horizontal cracks are smaller compared to the previous phase, however they remain open and their size depends on the level of residual plastic strain. It is assumed that the masonry contraction during this phase is negligible.

Subsequently, the specimen is reloaded in compression (path $b-c$), and the crack size is further reduced. During this phase, the reinforcing bars have to resist the entire applied compression load and provide stiffness in the lateral direction. As a result, the lateral stiffness is small and the entire specimen will start to move out-of-plane. This out-of-plane displacement causes rotation of the horizontal cracks (point c), which are shown in Figure 3.2b). Due to a single layer of longitudinal reinforcement placed in the hollow block cells, RM walls have higher potential for out-of-plane instability compared to RC walls or columns which usually have two layers of reinforcement and thus a better ability to resist high compression loads.

As the loading in compression continues along path $c-h$, the entire specimen will follow out-of-plane deformed shape of reinforcing bars until the cracks begin to close at one end, and the contact between the adjacent blocks is achieved (point d) before the wall becomes unstable. When the crack size and out-of-plane displacements are sufficiently small, internal compression forces will develop at the point of contact, thereby making the wall stiffer. The specimen will continue to restore its straightness with increased compression, thereby leading to the yielding of reinforcement in compression (point g). At the end of the compression half-cycle (point h), all cracks are closed and the entire cross-section is subjected to compression. The specimen maintains stability and the testing continues in compression.

Alternatively, the specimen can experience global out-of-plane instability in the form of two possible mechanisms. The first mechanism could be described as global out-of-plane instability combined with the localized masonry crushing at the location of maximum lateral displacement (path $b-c-d-e$). The specimen behaviour along path $b-c$ is the same as explained above. If the specimen experiences out-of-plane displacements that cause instability before the cracks close on one side (point d), it may continue to carry increased compressive loads and move laterally until local crushing takes place on one side (point e). The out-of-plane displacements leading to instability are generally equal to half the wall thickness ($t/2$) as discussed shortly and will be referred to as critical out-of-plane displacements hereafter. This is expected to occur at the point along the specimen height where the maximum lateral displacement has taken place. This mechanism is what was observed in specimens C2 through C4 in our experimental study. The second form of global out-of-plane instability corresponds to path $b-c-f$. This mechanism develops if the cracks at point c are very large, and it is not possible to restore contact at one end of the crack before or after critical out-of-plane displacements have occurred. Therefore, no further compressive stresses beyond what initiated the out-of-plane displacements are developed. (point f). Global out-of-plane instability in specimen C2 is illustrated in Figure 3.3. Axial load versus deformation diagram is shown in Figure 3.3a). It can be observed that hysteresis curves are similar in outline to the generic loading cycle presented in Figure 3.1. Deformed shape of the specimen at failure is shown in Figure 3.3b). These experimental results are typical of other tested specimens.

Note that the critical lateral displacement which causes the out-of-plane instability in a test specimen can be determined from the analysis of internal forces developed in the cracked wall section, when the cracks have rotated and significant lateral displacements have taken place (path $c-d$ shown in Figure 3.1). The lateral displacement, δ , is equal to the distance of the applied compression force from the centroid of the section, and it can be expressed in terms of the wall thickness, t and parameter ξ , that is, $\delta = \xi t$. Both masonry and steel are engaged in resisting the applied compression force. The masonry stress resultant acts over the compression zone, and steel resultant acts at the centroid of the section (location of longitudinal reinforcement). In the extreme case, the masonry compression zone

diminishes to a single point at the face of the specimen. As a result, the applied compression force acts at a distance $t/2$ from the resultant of steel force (centroid of the section). Therefore, the instability will take place when the maximum lateral displacement is equal to one-half of the wall thickness, that is, $\xi_{\max} = 0.5$.



Figure 3.2. Cracks in specimen C2: a) uniformly distributed horizontal cracks at bed joints (point *a'* on the load cycle), and b) rotated cracks (point *c* on the load cycle)

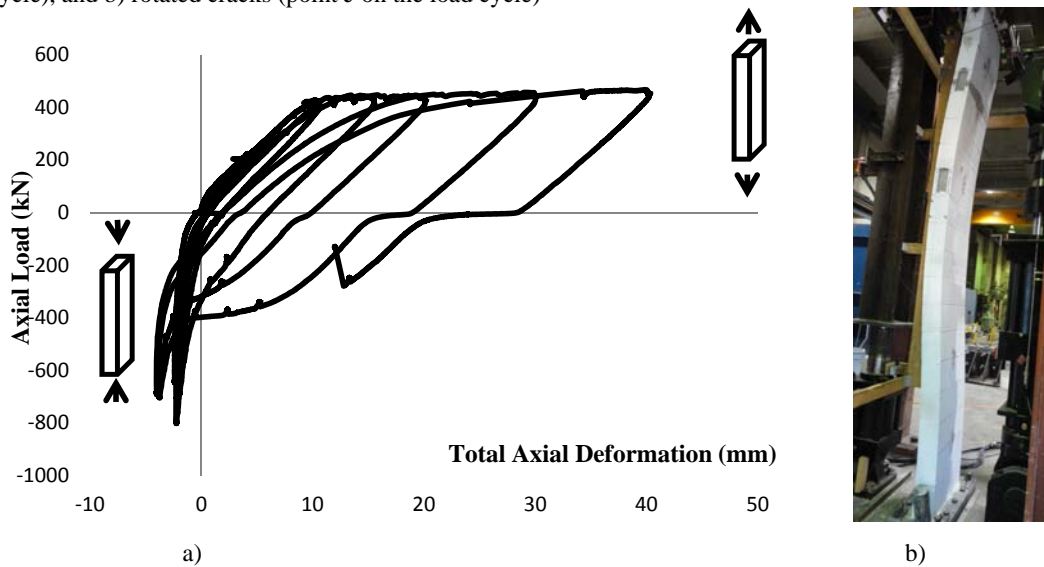


Figure 3.3. Global out-of-plane instability in specimen C2: a) axial load versus total axial deformation, and b) specimen C2 at the end of the test

Based on the observations made during this experimental study, it is concluded that the magnitude of the applied tensile strain is the primary factor in determining the potential for out-of-plane instability in the end zone of RM walls. This is because under monotonic compressive loads, lateral stiffness of the specimen is too large to allow considerable out-of-plane displacements prior to masonry crushing. Similarly, if the applied tensile strains do not cause sufficiently large cracks, the masonry compressive stresses will reverse any out-of-plane displacements that may have been experienced before the onset of instability. Therefore, a critical amount of tensile strain which causes large horizontal cracks is required to allow the specimen to experience lateral displacements beyond the critical values before the rotation of cracks results in crack closure on one face of the specimen. A secondary factor that seems to play a role in determining the failure mode is reinforcement size. Based on the results of tests on specimen C5, it is speculated that the small size of bars may result in severe

debonding between the rebar and the grout core which may mean that in the presence of large cracks, local buckling of reinforcement takes priority over global out-of-plane instability as a failure mode. An estimate of the bar size and reinforcement ratio that will determine the difference between the onset of these two failure mechanisms requires further investigation and analytical work.

4. STRAIN-BASED CRITERIA FOR PREDICTING OUT-OF-PLANE INSTABILITY IN RM SHEAR WALLS

Results of the Phase 1 study have shown that the tensile strain is the key parameter related to out-of-plane instability of RM shear walls subjected to combined gravity load and seismic overturning moment. An analytical model has been developed to estimate the magnitude of the critical tensile strain that leads to out-of-plane instability of RM specimens representing the end zone of a shear wall. The concept will be explained in this section, without detailed explanation of underlying theory and equations which were presented by Azimikor (2012).

The maximum tensile strain, ε_{sm} , can be expressed in the following form, which was originally proposed by Chai and Elayer (1999):

$$\varepsilon_{sm} = \varepsilon_e + \varepsilon_r + \varepsilon_p^* \quad (4.1)$$

The key strain components are explained below (see Figure 4.1):

1. ε_e is an elastic recovery strain (related to the unloading path **a'-b** shown in Figure 4.1). For an elastic-perfectly plastic tensile response, the ε_e would be equal to the yield strain. However, given that there may exist some strain hardening, the value of ε_e may be larger than yield strain.
2. ε_r is a reloading strain, which is needed, in addition to strain ε_e to cause critical out-of-plane displacement in the specimen. This strain is associated with out-of-plane displacement of longitudinal bars under small axial compressive loads up to the point of crack closure (path **b-d** on the loading cycle shown in Figure 4.1). The reloading strain can be estimated from a second order differential equation corresponding to the specimen's boundary conditions, using an idealized buckled shape of longitudinal bars.
3. ε_p^* is a residual plastic strain in rotated bed joints after the specimen has already experienced critical out-of-plane displacements. ε_p^* can be determined from one of the two possible approaches: i) based on an assumed bed joint rotation distribution (Model 1), and ii) based on an assumed curvature distribution with the maximum at midheight of the plastic hinge region (Model 2).

The key experimental results, including measured strains, and the corresponding values obtained from the analytical model, are presented in Table 4.1. It can be seen from the table that out-of-plane instability occurred at a lower level of applied axial tensile strain in specimens characterized by higher h/t value and reinforcement ratio (ρ). For example, specimen C2 which experienced instability at the lowest tensile strain of 0.79% was characterized by the largest plastic hinge height (h_p) of 3800 mm, and the highest reinforcement ratio ($\rho= 1.07\%$). A similar trend can be observed for specimen C3, which experienced instability at the strain of 0.80% was also characterized by relatively h_p and ρ values (3462 mm and 0.71% respectively). The remaining specimens (C4 and C5) achieved significantly higher tensile strains at failure (1.69 and 1.46% respectively), but they also had lower h_p and ρ values. Note that the maximum lateral displacements for all specimens (expressed in terms of the ξ_{max}) were in the range from 0.40 to 0.46; this is close to the theoretical critical value ($\xi_{max} = 0.5$)

A comparison of analytical and experimental strain values show that the analytical model discussed above was able to predict the strain values with a reasonable accuracy. Total strain values for Model 1 and Model 2 are different due to difference in the approach taken for estimating the strain ε_p^* , as discussed above. The proposed model could be used to develop a rational strain-based criterion for assessing potential for out-of-plane instability in RM shear walls for seismic design. The criterion should require that the inelastic tensile strain demand in the end zone of a RM shear wall, ε_{id} , should be less than the maximum tensile strain, ε_{sm} , which will lead to out-of-plane instability. The strain

demand ϵ_{id} can be determined for the given seismic design parameters, including the ductility level, wall dimensions, plastic hinge height, material and reinforcement properties.

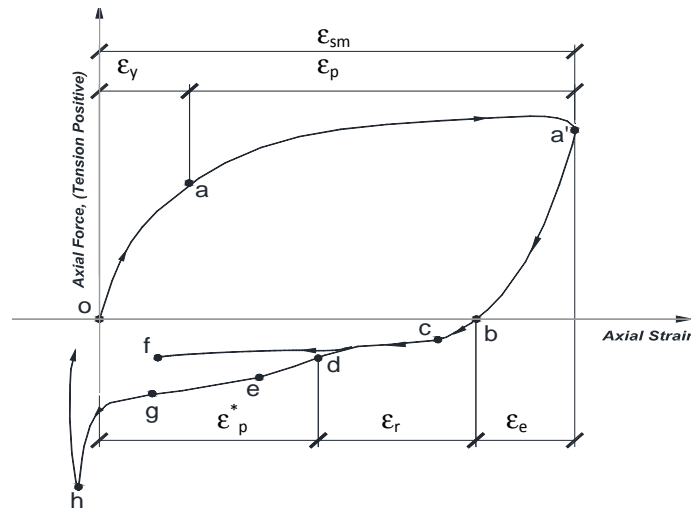


Figure 4.1. Tensile strain components

Table 4.1. Experimental and Analytical Tensile Strains: A Comparison

Specimen	h_p (mm)	ρ (%)	ξ_{max}	Tensile Strain components (%)									
				Experimental				Calculated					
				ϵ_e	ϵ_r	ϵ_p^*	ϵ_t	ϵ_e	ϵ_r	Model 1		Model 2	
										ϵ_p^*	ϵ_{sm}	ϵ_p^*	ϵ_{sm}
C2	3800	1.07	0.44	0.30	0.10	0.39	0.79	0.31	0.08	0.41	0.80	0.37	0.76
C3	3462	0.71	0.46	0.31	0.08	0.40	0.80	0.31	0.10	0.93	1.34	0.47	0.88
C4	2385	0.48	0.40	0.39	0.18	1.13	1.69	0.31	0.17	0.99	1.47	0.87	1.35
C5	2192	0.24	0.42	0.32	0.09	1.05	1.46	0.31	0.22	0.99	1.52	1.08	1.61

5. TESTING OF FULL-SCALE RM SHEAR WALL SPECIMENS UNDER REVERSED CYCLIC LOADING (PHASE 2)

Phase 2 of the research program involves experimental and analytical study of full-size RM shear walls subjected to reversed-cyclic lateral loading. The main objective is to develop a rational analysis procedure and criteria for assessing the out-of-plane stability of RM shear walls. The specimens represent the bottom storey of a midrise RM wall structure subjected to combined effects of axial stresses due to gravity loads, and lateral seismic forces and overturning moments. During the testing, the loads will be applied through a system of one displacement-controlled horizontal actuator and two force-controlled vertical actuators, which are intended to simulate the effect of overturning moments in a multi-storey building. The horizontal actuator will be supported by the strong wall, and an arrangement has been designed to prevent out-of-plane movement at the top of the specimen. The test setup is shown in Figure 5.1.

The current testing program comprises the four RM wall specimens. All specimens have the same dimensions: 3.8 m height, 2.6 m length, and 140 mm thickness; note that the height and thickness are the same for Phase 1 and Phase 2 specimens. Longitudinal reinforcement is continuous over the specimen height (no lap splices), and it consists of larger bar sizes placed in the two end cells (two 15M bars), and smaller bars (10M size) distributed along the specimen length. Horizontal reinforcement consists of 10M bars placed in bond beam blocks at each course. The first two specimens are fully grouted, however the effect of partial grouting may be considered in future. The specimens were designed in compliance with the CSA S304-04 seismic requirements for ductile RM walls. The first two specimens will be subjected to the same loading protocol, however different axial

stress levels will be applied ($0.07f'_m$ and $0.13f'_m$).

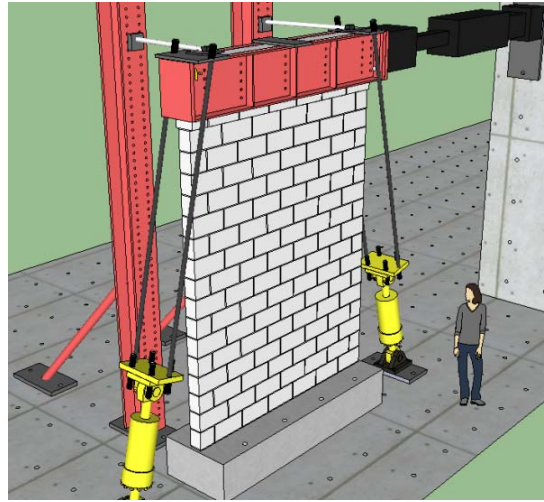


Figure 5.1. Test setup for Phase 2 experimental study

6. CONCLUSION

Results of the experimental study presented in this paper indicate that the magnitude of plastic tensile strain due to reversed cyclic tension and compression is the primary factor in determining the potential for out-of-plane instability in RM specimens simulating the end zone of a shear wall. A rational analytical model was developed to estimate the critical tensile strain corresponding to the onset of out-of-plane instability in RM shear walls.

ACKNOWLEDGEMENT

This research project has been sponsored by the Natural Sciences and Engineering Research Council of Canada (NSERC) under the Collaborative Research and Development Program, Canadian Concrete Masonry Producers Association and the Masonry Institute of British Columbia. The first and the second author acknowledge the support provided by the NSERC Industrial Postgraduate Scholarship program. The experimental testing would not be possible without the support provided by the UBC laboratory staff Scott Jackson and Blair Patterson, and Ken Zeleschuk, Assistant Instructor, BCIT Department of Civil Engineering. The authors acknowledge contribution of Porkeang Lim, undergraduate student at the BCIT Department of Civil Engineering, who participated in the Phase 1 experimental study through the NSERC Undergraduate Research Student Award.

REFERENCES

- Anderson, D., and Brzev, S. (2009). *Seismic Design Guide for Masonry Buildings*, Canadian Concrete Masonry Producers Association, Toronto, Ontario, 317 pp (www.ccmpa.ca).
- Azimikor, N. (2012). *Out-Of-Plane Stability Of Reinforced Masonry Shear Walls Under Seismic Loading: Cyclic Uniaxial Tests*, A Thesis Submitted in Partial Fulfillment of the Requirements for the Degree of Master of Applied Science in the Faculty of Graduate Studies (Civil Engineering), The University of British Columbia, 180 pp.
- Azimikor, N., Brzev, S., Elwood, K., and Anderson, D. (2011). *Out-of-Plane Stability of Reinforced Masonry Shear Walls*, Proceedings of the 11th North American Masonry Conference, Minneapolis, MN, USA.
- Chai Y. H. and Elayer D. T. (1999). Lateral Stability of Reinforced Concrete Columns under Axial Reversed Cyclic Tension and Compression [Journal] // *ACI Structural Journal*. - 1999. - pp. 780-789.
- Paulay, T. and Priestley, M.J.N. (1993). Stability of Ductile Structural Walls, *ACI Structural Journal*, Vol.90, No.4, pp.385-392.
- Priestley, N. J. and L. He (1992). *Seismic Behaviour of Flanged Masonry Shear Walls*. San Diego, Department of Applied Mechanics and Engineering Sciences, Univ. of California, 1992.
- Shedid, M. T., Drysdale, R.G., and El-Dakhkhni, W.W. (2008). Behaviour of Fully Grouted Reinforced Concrete Masonry Shear Walls in Flexure: Experimental Results. *Journal of Structural Engineering*, Vol, pp. 1754-1767.